Atomic Aftereffects and the Line Shape of Muonic X Rays*

P. Vogel
California Institute of Technology, Pasadena, California 91109
(Received 2 February 1973)

The muonic x-ray energy, by virtue of the electron screening, depends on the depletion of the electron states by Auger transitions and on the time needed for the refilling of the electron vacancies. The effect of these processes on the line shape of the muonic x rays is studied here. Equations for the electron $1s$-level population and for the muonic-x-ray center of gravity are derived and applied to representative examples of medium- and high-Z muonic atoms. It is shown that the atomic aftereffects (i.e., refilling of the $1s$ state) result in almost full screening in wide range of atomic numbers. The calculated energy shift with respect to the full screening is only 1–3 eV. The uncertainty, related to the uncertain width of the electron $1s$ vacancy is discussed and estimated.

INTRODUCTION

The muonic x-ray energy, by virtue of the electron screening, depends on the number of electrons in the $1s$ orbit. If a muonic transition starts while there is a $1s$ electron vacancy, its energy will depend on the time needed for refilling the vacancy by electrons from the higher orbits. Thus, the shape and the center of gravity of the muonic x-ray line depend on three processes: depletion of the electron states by the Auger transitions in the preceding stages of the muonic cascade, radiation and Auger widths of the initial muonic state and, finally, refilling of the $1s$ state by electrons from higher orbits.

The problem of the line shape of muonic x-rays is the subject of the present paper. An analogous problem was briefly discussed by Kankeleit and Körding,[1] but, to our knowledge, it was never solved quantitatively.

Accurate muonic x-ray energy measurements were recently used for tests of the quantum electrodynamics[2,3]; similar experiments with higher accuracy are planned at the new high-intensity accelerators. Good knowledge of all corrections, including those related to the dynamical aspects of the electron screening, is essential for a meaningful interpretation of the experimental results.

The electron-screening corrections to the muon binding energy were discussed in a number of recent papers.[4–6] The electron density and its potential were calculated self-consistently, using the relativistic Hartree-Fock-Slater method. The results of Refs. 4–6 agree well with each other and with the scant experimental evidence. They are used here as a basis for a more detailed investigation of the muonic x-ray line shape. The calculations are restricted to the $1s$ electrons, which account for about 85% of the total screening. The rest, caused by higher electron orbits, depends more sensitively on the unknown initial stages of the muonic cascade.

Atomic transitions, induced by processes (decays, transitions, etc.) occurring at or near the nucleus are referred to as aftereffects. Refilling of the electron vacancies, formed during the muonic cascade, is an example of this phenomenon. It is shown here, that aftereffects have a measurable influence on the properties of muonic x-rays.

LINE SHAPE OF MUONIC X RAYS

General theory of the damping phenomena is described, for example, in Heitler's monograph.[7] The energy distribution (i.e., the line shape) of the emitted radiation is given by

$$w(k) = \sum_{\lambda} |b_{\lambda,k}(\infty)|^2 , \tag{1}$$

where $b_{\lambda,k}(\infty)$ is the amplitude of the corresponding wave function, taken at time $t=\infty$, and λ symbolically denotes all unobserved degrees of freedom.

Let us apply the general formalism to the part of the muonic cascade shown in Fig. 1. Assume that at $t=0$ the muon is in the state 0 and there is only one electron present in the $1s$ orbit. Each step $(0\to f,\ f\to g)$ proceeds by radiation or Auger K-electron emission; the transition energy $E^{(i)}_{0\to f}$ depends, through screening, on the number i of the bound $1s$ electrons present during the transition. The general wave function of the system has the form

$$|\mu; (1s)^i; k_\mu^{(1)}, k_\mu^{(2)}, \ldots; q^{(1)}, q^{(2)}, \ldots; \eta^{(1)}, \eta^{(2)}, \ldots\rangle . \tag{2}$$

Here μ describes the state of the muon, $(1s)^i$ the state of the bound $1s$ electrons. The $k_\mu^{(1)}, k_\mu^{(2)}, \ldots$ are photons with energies close to the muonic transition energies; $q^{(1)}$, $q^{(2)}, \ldots$ describe free

Auger electrons; and $\eta^{(1)}, \eta^{(2)}, \ldots$ describe photons with energies close to the electronic x-ray transition energies.

When calculating the amplitudes $b_n(\infty)$, several approximations are made: The level displacements are neglected, i.e., the level widths are real numbers; the interaction matrix elements and the corresponding final-state densities depend weakly on energy (in an energy interval equal to the level width).

Taking the square of $b_n(\infty)$ and integrating through all directions and momenta of the unobserved quanta, the following spectral shape of the $0 \to f$ x-ray is obtained (for details see the appendix):

$$w(k) = \frac{\gamma_R^0 (T^0 + T^f)}{T^0} \frac{1}{(k - E_{0\to f}^{(1)})^2 + \frac{1}{4}(T^0 + T^f)^2} + \frac{\gamma_R^0 \gamma_X (\Gamma^0 + \Gamma^f)}{T^0 \Gamma^f} \frac{1}{(k - E_{0\to f}^{(2)})^2 + \frac{1}{4}(\Gamma^0 + \Gamma^f)^2} . \tag{3}$$

Here

$$\Gamma^j = \gamma_R^j + \gamma_A^j, \quad T^j = \gamma_R^j + \tfrac{1}{2}\gamma_A^j + \gamma_X, \quad G^j = \gamma_R^j + 2\gamma_X , \tag{4}$$

and $\gamma_R^j (\gamma_A^j)$ are radiation (Auger) widths of the state j; γ_A^j corresponds to two $1s$ electrons. The γ_X is the total width of one electron vacancy in the $1s$ orbit.

As expected, the spectrum consists of two Lorentzians centered at $E_{0\to f}^{(1)}$ and $E_{0\to f}^{(2)}$. Their areas are

$$w(E^{(2)}) = \frac{\gamma_X \gamma_R^0}{T^0 \Gamma^0}, \quad w(E^{(1)}) = \frac{\gamma_R^0}{T^0} . \tag{5}$$

The meaning of Eqs. (5) becomes obvious if we realize that γ_R^0/T^0 and γ_X/T^0 are the probabilities of the competing muonic and electronic transitions, respectively; γ_R^0/Γ^0 is the muonic transition probability after an electron x-ray emission.

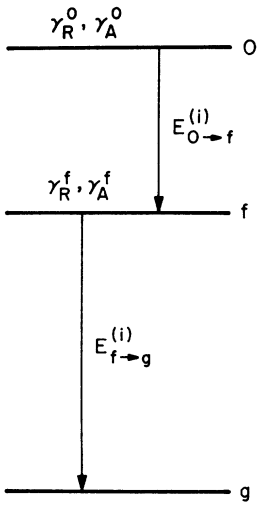

FIG. 1. Part of the muonic cascade discussed in the text. $E_{0\to f}^{(i)}$ is the transition energy, which depends on the number i of $1s$ electrons present during the transition. The γ_R (γ_A) are the radiation (Auger K-electron) widths.

From Eqs. (5) the Auger transition rate $\gamma_A^{0\prime}$ corrected for repopulation of the electronic $1s$ state can be calculated.[8] It is

$$w(E^{(1)}) + w(E^{(2)}) = \gamma_R^0/(\gamma_A^{0\prime} + \gamma_R^0), \qquad \gamma_A^{0\prime} = \tfrac{1}{2}\gamma_A^0 \frac{\gamma_R^0 + \gamma_A^0 + 2\gamma_X}{\gamma_R^0 + \gamma_A^0 + \gamma_X} . \tag{6}$$

Let us, for completeness, give several more equations. If, at time $t = 0$, the muon is in state 0 and the $1s$ electron orbit is completely empty, the corresponding muonic x-ray line consists of three Lorentzians:

TABLE I. Transitions between spherical orbits in muonic $^{92}_{42}$Mo. Total screening effect of all $Z-1$ electrons is shown in column 2. Column 3 gives the screening effect of one $1s$ electron, defined in Eq. (10). Total intensity of the muonic x ray, per captured muon, is shown in column 4. Columns 5, 6, and 7 give total width (for fully occupied electron shells), the radiation width, and the Auger K-electron width, respectively, for the initial state of the transition. For each of the $1s$ electron widths γ_X, given in the first line, the following values are shown: δE— shift of the center of gravity of muonic x ray, Eq.(11); a_2—probability of having two $1s$ electrons initially; and a_1—probability of having one $1s$ electron initially (note: $a_0 = 1 - a_2 - a_1$).

							$\gamma_X = 4.15$ eV			$\gamma_X = 2.08$ eV			$\gamma_X = 0.04$ eV		
Transition	E_{scr} (eV)	ΔE_{scr} (eV)	w (%)	Γ (eV)	γ_R (eV)	γ_A (eV)	δE (eV)	a_2 (%)	a_1 (%)	δE (eV)	a_2 (%)	a_1 (%)	δE (eV)	a_2 (%)	a_1 (%)
$9l_{17/2} \to 8k_{15/2}$	−72	−31	5	0.4	0.1	···	0.5	80	20	1.0	80	20	6.2	78	22
$8k_{15/2} \to 7i_{13/2}$	−57	−25	2	1.3	0.2	1.0	0.9	86	14	1.6	85	15	10.6	71	28
$7i_{13/2} \to 6h_{11/2}$	−44	−19	7	1.0	0.3	0.6	2.9	24	75	5.1	23	74	20.8	18	65
$6h_{11/2} \to 5g_{9/2}$	−31	−13	14	1.1	0.8	0.3	1.8	39	57	3.3	36	56	16.1	15	48
$5g_{9/2} \to 4f_{7/2}$	−20	−9	23	2.1	2.0	0.1	1.0	68	30	1.9	62	34	10.6	18	45
$4f_{7/2} \to 3d_{5/2}$	−11	−5	34	6.5	6.5	0.0	0.5	86	13	0.8	79	20	5.4	23	45

TABLE II. Transitions between spherical orbits in muonic $^{138}_{56}$Ba (see caption of Table I).

Transition	E_{scr} (eV)	ΔE_{scr} (eV)	w (%)	Γ (eV)	γ_R (eV)	γ_A (eV)	$\gamma_X = 12.0$ eV: δE (eV)	a_2 (%)	a_1 (%)	$\gamma_X = 6.0$ eV: δE (eV)	a_2 (%)	a_1 (%)	$\gamma_X = 0.12$ eV: δE (eV)	a_2 (%)	a_1 (%)
$9l_{17/2} \rightarrow 8k_{15/2}$	−105	−46	8	0.6	0.3	···	0.4	84	16	0.7	84	16	6.9	82	18
$8k_{15/2} \rightarrow 7i_{13/2}$	−86	−37	5	1.7	0.5	1.0	0.5	90	10	0.9	90	10	10.1	79	20
$7i_{13/2} \rightarrow 6h_{11/2}$	−66	−28	11	1.7	1.0	0.6	2.0	43	56	3.6	43	56	20.6	36	56
$6h_{11/2} \rightarrow 5g_{9/2}$	−47	−20	19	2.6	2.2	0.3	1.3	64	35	2.4	62	36	16.4	33	51
$5g_{9/2} \rightarrow 4f_{7/2}$	−31	−13	28	5.9	5.7	0.1	0.6	85	15	1.3	81	18	9.9	38	47
$4f_{7/2} \rightarrow 3d_{5/2}$	−18	−8	38	18.6	18.6	0.0	0.3	94	6	0.6	90	10	5.6	42	45

$$w(k) = \frac{\gamma_R^0}{G^0} \frac{G^0 + G^f}{(k - E^{(0)}_{0\rightarrow f})^2 + \frac{1}{4}(G^0 + G^f)^2} + \frac{2\gamma_X\gamma_R^0}{T^0 G^0} \frac{T^0 + T^f}{(k - E^{(1)}_{0\rightarrow f})^2 + \frac{1}{4}(T^0 + T^f)^2} + \frac{2\gamma_X\gamma_X\gamma_R^0}{T^0\Gamma^0 G^0} \frac{\Gamma^0 + \Gamma^f}{(k - E^{(2)}_{0\rightarrow f})^2 + \frac{1}{4}(\Gamma^0 + \Gamma^f)^2} . \quad (7)$$

In the general case, the population of the electron $1s$ orbit is characterized by three probabilities, $a_0^{(0)}$, $a_1^{(0)}$, and $a_2^{(0)}$ (empty, one, and two electrons) at time $t = 0$. The population of the electron $1s$ orbit, when the muon has reached state f, is characterized by probabilities $a_0^{(f)}$, $a_1^{(f)}$, and $a_2^{(f)}$. It is

$$a_0^{(f)} = \frac{a_0^{(0)}}{G^0}\left(\gamma_R^0 + \frac{\gamma_X\gamma_A^0}{T^0}\right) + \frac{a_1^{(0)}\gamma_A^0}{2T^0}, \quad (8a)$$

$$a_1^{(f)} = \frac{2a_0^{(0)}\gamma_X}{T^0 G^0}\left(\gamma_R^0 + \frac{\gamma_X\gamma_A^0}{\Gamma^0}\right) + \frac{a_1^{(0)}}{T^0}\left(\gamma_R^0 + \frac{\gamma_X\gamma_A^0}{\Gamma^0}\right) + \frac{a_2^{(0)}\gamma_A^0}{\Gamma^0}, \quad (8b)$$

$$a_2^{(f)} = \frac{2a_0^{(0)}\gamma_X\gamma_X\gamma_R^0}{T^0\Gamma^0 G^0} + \frac{a_1^{(0)}\gamma_X\gamma_R^0}{T^0\Gamma^0} + \frac{a_2^{(0)}\gamma_R^0}{\Gamma^0} . \quad (8c)$$

The center of gravity of the muonic $0 \rightarrow f$ x ray is in the general case given by

$$\bar{E}_{0\rightarrow f} = \left[\left(a_2^{(0)} + a_1^{(0)}\frac{\gamma_X}{T^0} + a_0^{(0)}\frac{2\gamma_X\gamma_X}{T^0 G^0}\right)\frac{E^{(2)}_{0\rightarrow f}}{\Gamma^0} + \left(a_1^{(0)} + a_0^{(0)}\frac{2\gamma_X}{G^0}\right)\frac{E^{(1)}_{0\rightarrow f}}{T^0} + a_0^{(0)}\frac{E^{(0)}_{0\rightarrow f}}{G^0}\right] \Big/ I , \quad (9)$$

where

$$I = \frac{a_2^{(0)}}{\Gamma^0} + \left(1 + \frac{\gamma_X}{\Gamma^0}\right)\frac{a_1^{(0)}}{T^0} + \left(1 + \frac{2\gamma_X}{T^0} + \frac{2\gamma_X\gamma_X}{T^0\Gamma^0}\right)\frac{a_0^{(0)}}{G^0} .$$

RESULTS AND DISCUSSION

The equations of the preceding section were applied to representative medium- and large-Z muonic atoms. The most intense transitions between spherical orbits were calculated. Tables I–IV show the results for $Z = 42$, 56, 69, and 82.

A "standard" muonic cascade calculation[9] was modified to take into account the refilling of the electron $1s$ orbit. [Trivial generalization of Eqs. (3)–(9), which includes branchings in the cascade, was used for the numerical calculation.] The cascade started at $n = 15$, whereby the $1s$ electron shell is fully occupied. (Muon binding energy is smaller than the $1s$ electron binding for $n \geq 15$.)

Statistical population [i.e., population proportional to $(2l + 1)$] was assumed at $n = 15$. The nonrelativistic expressions for the radiation rates and the full K and L Auger rates from Ref. 9 were employed. The K-electron Auger rates were, at each step, corrected according to Eq. (6). The bookkeeping of the electron ($1s$) level population was done according to Eqs. (8a)–(8c). The Auger L rates were simply reduced in proportion to the number of the L electrons present.

The electron screening was treated according to method II of Ref. 5; the self-consistent poten-

TABLE III. Transitions between spherical orbits in muonic $^{169}_{69}$Tm (see caption of Table I).

Transition	E_{scr} (eV)	ΔE_{scr} (eV)	w (%)	Γ (eV)	γ_R (eV)	γ_A (eV)	$\gamma_X = 27.5$ eV: δE (eV)	a_2 (%)	a_1 (%)	$\gamma_X = 13.8$ eV: δE (eV)	a_2 (%)	a_1 (%)	$\gamma_X = 0.27$ eV: δE (eV)	a_2 (%)	a_1 (%)
$9l_{17/2} \rightarrow 8k_{15/2}$	−155	−65	10	0.9	0.6	···	0.0	98	2	0.1	98	2	1.0	98	2
$8k_{15/2} \rightarrow 7i_{13/2}$	−128	−54	8	2.3	1.1	1.0	0.3	93	7	0.6	93	7	4.7	92	8
$7i_{13/2} \rightarrow 6h_{11/2}$	−101	−42	16	3.0	2.3	0.6	1.6	62	38	2.9	62	38	17.2	59	40
$6h_{11/2} \rightarrow 5g_{9/2}$	−75	−32	24	5.4	5.1	0.3	1.1	80	19	2.1	78	21	14.6	57	39
$5g_{9/2} \rightarrow 4f_{7/2}$	−50	−21	33	13.3	13.2	0.1	0.6	92	7	1.0	90	10	9.5	59	36
$4f_{7/2} \rightarrow 3d_{5/2}$	−30	−13	43	42.7	42.7	0.0	0.2	97	3	0.5	95	5	5.6	62	33

TABLE IV. Transitions between spherical orbits in muonic $^{208}_{82}$Pb (see caption of Table I).

Transition	E_{scr} (eV)	ΔE_{scr} (eV)	w (%)	Γ (eV)	γ_R (eV)	γ_A (eV)	$\gamma_X = 54.8$ eV: δE (eV)	a_2 (%)	a_1 (%)	$\gamma_X = 27.4$ eV: δE (eV)	a_2 (%)	a_1 (%)	$\gamma_X = 0.55$ eV: δE (eV)	a_2 (%)	a_1 (%)
$9l_{17/2} \rightarrow 8k_{15/2}$	−228	−91	12	1.5	1.3	...	0.0	99	1	0.0	99	1	0.7	99	1
$8k_{15/2} \rightarrow 7i_{13/2}$	−193	−80	12	3.5	2.3	1.0	0.2	96	4	0.4	96	4	3.9	95	5
$7i_{13/2} \rightarrow 6h_{11/2}$	−159	−65	20	5.3	4.6	0.6	1.4	75	25	2.7	75	25	17.2	73	26
$6h_{11/2} \rightarrow 5g_{9/2}$	−121	−47	27	10.5	10.2	0.3	0.8	89	11	1.8	87	12	13.1	72	27
$5g_{9/2} \rightarrow 4f_{7/2}$	−86	−39	36	26.4	26.3	0.1	0.5	96	4	1.1	94	6	10.3	74	25
$4f_{7/2} \rightarrow 3d_{5/2}$	−53	−21	45	85.1	85.1	0.0	0.3	98	2	0.5	97	3	5.2	76	23

tial of $(Z-1)$ electrons is added to the nuclear potential in the muon Dirac equation. The resulting full-screening correction E_{scr} is given in the second column of Tables I – IV. The third column of Tables I–IV gives the screening effect of one $1s$ electron, i.e.,

$$\Delta E_{scr} \equiv E^{(2)}_{0\rightarrow f} - E^{(1)}_{0\rightarrow f} \simeq E^{(1)}_{0\rightarrow f} - E^{(0)}_{0\rightarrow f} . \quad (10)$$

With refilling of the electron $1s$ orbit, the muonic cascade depends on the width γ_X of the one-electron vacancy in the $1s$ state. For normal atoms this quantity is well known (see, e.g., Ref. 10). The higher electron orbits of a muonic atom are, however, strongly depleted during the cascade. Therefore, the real γ_X is considerably smaller than γ_X of a normal atom. It is impossible to calculate the γ_X in muonic atoms precisely, as there are no accurate theories of the early stages of the cascade.

The present calculations were done for three values of γ_X: (a)γ_X of a "normal" atom according to Ref. 10; (b) half of the value (a)—this is probably close to the realistic value; (c) 1% of the value (a)—this is unrealistically small, the refilling being unimportant then. Our calculations show that two to four $2p$ or $2s$ electrons are released in the cascade between $n=15$ and $n=7$. Assuming that about the same number are released for $n>15$, we come to our rough estimate of γ_X. The total intensity of the muonic x ray does not depend critically on the γ_X value. Therefore, only one value is shown in column four of Tables I–IV.

For each value of γ_X, Tables I–IV give the calculated shift δE of the center of gravity of the muonic x ray. This quantity is defined as

$$\delta E = \bar{E}_{0\rightarrow f} - E^{(2)}_{0\rightarrow f} , \quad (11)$$

i.e., the difference between the real screening and the full screening.

Figures 2 and 3 show the calculated line shape for two of the most strongly affected transitions. It is seen that the peak at $E^{(2)}$ is overwhelming for large, realistic γ_X values. It is important to remember that ΔE_{scr}, Eq. (10), is smaller than the instrumental linewidth, even for curved-crystal spectrometers. Thus, the observable line profile

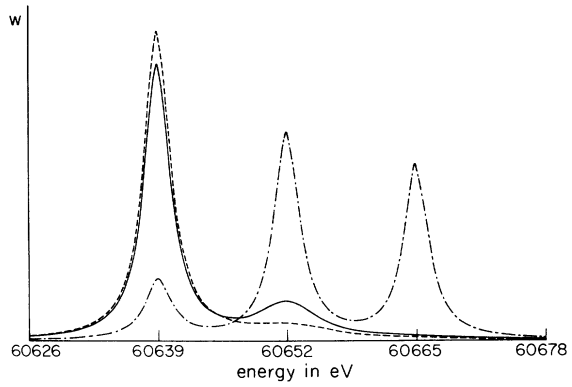

FIG. 2. Line shape of the $6h_{11/2} \rightarrow 5g_{9/2}$ transition in muonic $^{96}_{42}$Mo. The three curves correspond to three values of the $1s$ electron width γ_X: dashed curve, $\gamma_X = 4.15$ eV; full curve, $\gamma_X = 2.08$ eV; dot-dashed curve, $\gamma_X = 0.04$ eV. The peaks are at $E^{(2)} = 60639$ eV, $E^{(1)} = 60652$ eV, $E^{(0)} = 60665$ eV; these values were calculated without the quantum-electrodynamic and nuclear-polarization corrections.

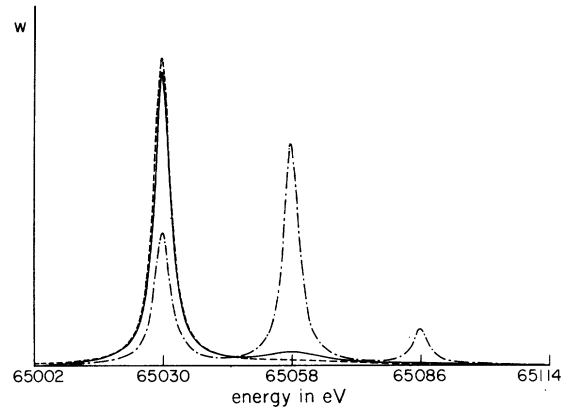

FIG. 3. Line shape of the $7i_{13/2} \rightarrow 6h_{11/2}$ transition in muonic $^{138}_{56}$Ba. As in Fig. 2, three values of γ_X were used: dashed curve, $\gamma_X = 12.0$ eV; full curve, $\gamma_X = 6.0$ eV; dot-dashed curve, $\gamma_X = 0.12$ eV. The peaks are at $E^{(2)} = 65030$ eV, $E^{(1)} = 65058$ eV, $E^{(0)} = 65086$ eV.

is the natural line folded into a Gaussian instrumental line shape. The presence of the $E^{(1)}$ and $E^{(0)}$ parts of the line will cause an asymmetry of the resulting observable line.

The calculations clearly show the diminishing role of Auger transitions, and thus also aftereffects, with increasing atomic number Z; this is a well-known effect. The most important quantity for practical application is the center-of-gravity shift δE. The calculations show that for realistic γ_x values, the aftereffects (i.e., refilling of the electron 1s state) substantially reduce the δE value. Practically full screening effect is expected even for medium-Z muonic atoms. For the accurately measured $5g \rightarrow 4f$ transition in Pb,[2] the expected shift is only 1 eV, compared with the full screening of −86 eV. The $6h \rightarrow 5g$ transition in $_{42}$Mo and the $7i \rightarrow 6h$ transition in $_{56}$Ba might be soon accessible to measurements with curved-crystal spectrometers; the expected shift there is about 3 eV. While it is unlikely that such measurements could be used for the γ_x determination,[11] they would undoubtedly discriminate between the extreme cases shown in the tables (i.e., difference about 15 eV).

Using the present calculations, the uncertainty in the muonic transition energy, related to the uncertain γ_x value, is seen to be about 1 eV. This value is smaller than (or comparable with) the uncertainty in the total screening correction, related to the approximations used in calculating the electron self-consistent potential. It should be remembered, however, that the screening contribution of the higher electron orbits (about 15% of the total screening effect) is affected by the aftereffects as well, thus increasing the uncertainty in the muonic x-ray energy.

APPENDIX

The derivation of the basic equation (3) is briefly described here. According to Ref. (7), the amplitude $b_\lambda(\infty)$ in Eq. (1) is equal to (we use the $\hbar = 1$ system of units)

$$b_\lambda(\infty) = \frac{U_\lambda(E_\lambda)}{E_\lambda - E_0 + \frac{1}{2} i \Gamma(E_\lambda)} . \tag{A1}$$

The functions $U_\lambda(E)$ are solutions of the system

$$U_\lambda(E) = \langle \lambda | H | 0 \rangle + \sum_{\lambda' \neq 0} \langle \lambda | H | \lambda' \rangle U_{\lambda'}(E) \xi(E - E_{\lambda'}), \quad \lambda \neq 0 \tag{A2}$$

and the full width $\Gamma(E)$ is determined by

$$\tfrac{1}{2}\Gamma(E) = i \left(\langle 0 | H | 0 \rangle + \sum_{\lambda' \neq 0} \langle 0 | H | \lambda' \rangle U_{\lambda'}(E) \xi(E - E_{\lambda'}) \right) . \tag{A3}$$

The Hamiltonian H describes the interaction of the charged particles with the radiation field; E_λ is the total energy of the state λ; and E_0 is the energy of the initial state. As usual,

$$\xi(x) = P/x - i\pi\delta(x) . \tag{A4}$$

First, the system of Eqs. (A2) must be solved for the situation shown in Fig. 1. Obviously

$$U_g(E) = \langle g | H | f \rangle U_f(E) \xi(E - E_f) , \tag{A5}$$

i.e., the equation for $U_g(E)$ corresponding to the final state has only one right-hand-side term. This fact, together with the standard definitions of the partial widths collected in Eq. (4) and with the known properties of the function $\xi(x)$ is used to obtain the expressions for the corresponding amplitudes. Such a procedure is straightforward, but lengthy.

There are several amplitudes relevant to our process: The electronic x-ray may either precede the $0 \rightarrow f$ muonic transition, which can proceed via radiation or Auger emission [these processes give the second term in Eq. (3)], or the $0 \rightarrow f$ muonic transition may proceed first [such a process gives the first term in Eq. (3)].

For example, the amplitude for the emission of the electronic x-ray, followed by the two muonic x rays (i.e., only radiative processes) is equal to

$$b_g(\infty) = \frac{\langle g | H | f \rangle}{k^{(2)} - E^{(2)}_{f \rightarrow g} + \frac{1}{2} i \Gamma^f} \frac{\langle f | H | 0 \rangle}{k^{(2)} + k - E^{(2)}_{f \rightarrow g} - E^{(2)}_{0 \rightarrow f} + \frac{1}{2} i \Gamma^0} \times \frac{\langle s^{(2)} | H | s^{(1)} \rangle}{k^{(2)} + k + k_x - E^{(2)}_{f \rightarrow g} - E^{(2)}_{0 \rightarrow f} - E_x + \frac{1}{2} i \Gamma^0} \tag{A6}$$

where $\langle s^{(2)} | H | s^{(1)} \rangle$ is the matrix element of the electronic x-ray emission; k_x, k, $k^{(2)}$ are momenta of the emitted electronic x ray and $0 \rightarrow f$ and $f \rightarrow g$ muonic x rays, respectively. Other symbols have been explained previously.

As the final step, it is necessary to integrate $|b_\lambda(\infty)|^2$ over the unobserved quanta [i.e., over $d^3k^{(2)}$ and d^3k_x in the case (A6) above], and over all directions of the $0 \rightarrow f$ radiation. This is again simple if the Cauchy theorem is used. Adding all contributions together we obtain, finally, Eq. (3).

---

*Work performed under the auspices of the U. S. Atomic Energy Commission under Contract No. AT (04-3)-63.

[1]E. Kankeleit and A. Körding, in *Hyperfine Structure and Nuclear Radiation*, edited by E. Matthias and D. A. Shirley (North-Holland, Amsterdam, 1968).

[2]M. S. Dixit *et al.*, Phys. Rev. Lett. 27, 878 (1971).

[3]H. K. Walter *et al.*, Phys. Lett. B 40, 197 (1972).

[4]B. Fricke, Nuovo Cimento Lett. 2, 859 (1969).

[5]P. Vogel, Phys. Rev. A 7, 63 (1973).
[6]B. Fricke, J. T. Waber, and V. L. Telegdi (report of work prior to publication, 1972).
[7]W. Heitler, *The Quantum Theory of Radiation* (Clarendon, Oxford, England, 1954).
[8]Note that Eq. (6) can also be obtained starting simply with the classical equation $dn_0/dt = -T^0 n_0$, [and analgous equations for the other states (2)]. A formula equivalent to (6) was used in Ref. 5. The classical equations were used consistently and the Auger rate was treated as a continuous function of time. (It has only two possible values, γ_A^0 and $\frac{1}{2}\gamma_A^0$, in the quantized theory here). Although Eq. (6) and Eq. (A5) of Ref. 5, which contains the integral of doubly exponential function, look entirely different, they give essentially identical numerical results.
[9]Y. Eisenberg and D. Kessler, Nuovo Cimento 19, 1195 (1961).
[10]W. Bambynek *et al.*, Rev. Mod. Phys. 66, 716 (1972).
[11]The energy of the electron x ray, emitted during refilling of the 1*s* vacancy, depends on the γ_X value as well. This effect was discussed, e.g., in Ref. 5.